Solar Energy Materials & Solar Cells 123 (2014) 112–121

Contents lists available at ScienceDirect

Solar Energy Materials & Solar Cells

journal homepage: www.elsevier.com/locate/solmat

Correlation of intramolecular charge transfer and orientation properties among quinacridone and acceptor units

Ho Jun Song [a,b], Doo Hun Kim [a], Eui Jin Lee [a], Jung Rim Haw [a], Doo Kyung Moon [a,*]

[a] Department of Materials Chemistry and Engineering, Konkuk University, 1 Hwayang-dong, Gwangjin-gu, Seoul 143-701, Republic of Korea
[b] Cungcheong Regional Division IT Convergence Material R&D Group, Korea Institute of Industrial Technology, 89 Yangdaegiro-gil, Ipjang-myeon, Seobuk-gu, Cheonan-si, Chungcheongnam-do 331-822, Republic of Korea

ARTICLE INFO

Article history:
Received 15 October 2013
Received in revised form
2 December 2013
Accepted 8 December 2013
Available online 1 February 2014

Keywords:
Quinacridone
Self-organization
OPVs
Conjugated polymer

ABSTRACT

This study synthesized a highly soluble quinacridone-acceptor series (PQCDTB, PQCDTQ-a, PQCDTQ-b) through the Suzuki coupling reaction by introducing planar quinacridone and a highly soluble acceptor unit. The polymers largely dissolved organic solvents, and the M_n ranged from 40.5 to 63.1 kg/mol. The intermolecular charge transfer (ICT) effects were much stronger in PQCDTQ-b than in PQCDTB and PQCDTQ due to the position of the oxygen atom. The HOMO and LUMO levels of the polymers were −5.18 to −5.37 eV and −3.28 to −3.40 eV, respectively. According to XRD measurements, PQCDTB exhibited the formation of an ordered lamellar structure and conventional edge-on π-stacking, whereas PQCDTQ-a and PQCDTQ-b exhibited face-on formation relative to the substrate. The open-circuit voltage (V_{OC}), short-circuit current (J_{SC}), fill factor (FF), and power conversion efficiency (PCE) were 0.85 V, 7.6 mA/cm^2, 61.5%, and 4.0%, respectively, for PQCDTQ-a with a 1:2 ratio of $PC_{71}BM$.

1. Introduction

Semiconducting polymers have been used in diverse applications, such as organic light emitting diodes (OLEDs) [1–3], organic photovoltaic cells (OPVs) [4–11], and organic thin film transistors (OTFTs) [12,13], for several decades. OPVs have received significant attention in these applications due to the global technology trend toward economic feasibility and continuous development coupled with preservation of the environment. However, the low power conversion efficiency (PCE) of these materials has been the greatest obstacle in developing OPVs [6]. The donor–acceptor (D–A)-type low-band gap polymer has received considerable attention in recent years because its electronic properties can easily be changed based on the unique combination of the D–A unit. This polymer can also increase the absorption spectra with long wavelengths [6]. Nevertheless, the low PCE has remained the largest obstacle in D–A-type polymers.

The following idealistic conditions are required in D–A-type polymers to improve the PCE [14]: (1) a low band gap with a wide absorption area, (2) ordered orientation to produce good charge transport characteristics, (3) a low highest occupied molecular orbital (HOMO) energy level with which a high open-circuit voltage (V_{OC}) can be produced, and (4) an appropriate lowest unoccupied molecular orbital (LUMO) energy level for effective electron charge transfer to fullerene.

To acquire good charge transport characteristics, the close packing between polymers must be increased through the reduction of energetic disorder by increasing the coplanarity and interchain π–π interaction. A quinacridone (QC) derivative is an appropriate candidate for this process. A QC derivative, which is known as a red-violet pigment, has an ordered structure and self-assembled characteristics and has received significant attention as an OTFT because of its high mobility [15,16]. The Takimiya group has recently reported on a polymer composed of QC derivatives with a high hole mobility (0.2 cm^2 V^{-1} S^{-1}) for use in OTFTs [17]. We have synthesized polymers by introducing QC, benzothiadiazole, and a quinoxaline derivative and reported on the optical, electrochemical, and photovoltaic properties [18,19].

As observed in Chart 1, the polymer structure with oxygen around the backbone exhibits a weak intramolecular charge transfer (ICT) effect due to the electro-deficient property of the oxygen atom, which will exhibit a wide band gap and high LUMO level [20]. In addition, for the quinoxaline derivative, a polymer with quinoxaline exhibits various electrochemical and morphology properties depending on the position of the alkoxy chain [21]. Thus, if the oxygen position is far away around the polymer backbone, the polymer will exhibit an effective ICT effect and a broader absorption.

In this study, we synthesized D–A-type polymers based on a QC derivative depending on the oxygen position, and the resulting optical, electrochemical, and morphology properties were investigated. In

* Corresponding author. Tel.: +82 2 450 3498; fax: +82 2 444 0765.
E-mail address: dkmoon@konkuk.ac.kr (D.K. Moon).

0927-0248/$ - see front matter © 2013 Elsevier B.V. All rights reserved.
http://dx.doi.org/10.1016/j.solmat.2013.12.004

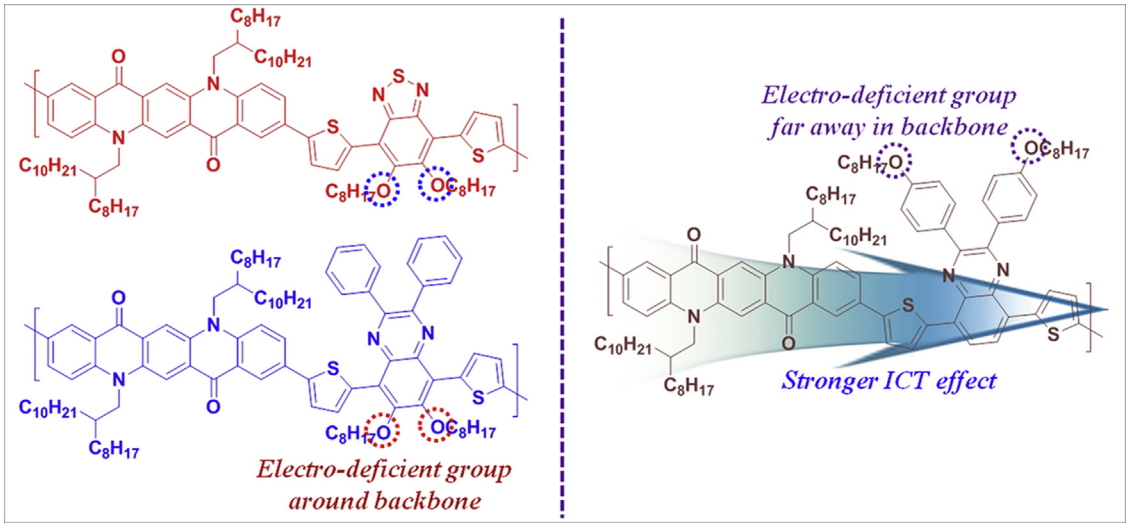

Chart 1. Schematic representation of effective intramolecular charge transfer.

addition, polymers based on a QC derivative reported by our group revealed improved efficiency through optimized device structure (additive, solvent) compared with the previously reported efficiency.

2. Experimental

2.1. Instruments and characterization

Unless otherwise specified, all the reactions were carried out under nitrogen atmosphere. Solvents were dried by standard procedures. All column chromatography was performed with the use of silica gel (230–400 mesh, Merck) as the stationary phase. ^{1}H NMR spectra were performed in a Bruker ARX 400 spectrometer using solutions in CDCl3 and chemical were recorded in ppm units with TMS as the internal standard. The elemental analyses were measured with EA1112 using a CE Instrument. Electronic absorption spectra were measured in chloroform using a HP Agilent 8453 UV–vis spectrophotometer. The cyclic voltammetric waves were produced using a Zahner IM6eX electrochemical workstation with a 0.1 M acetonitrile (substituted with nitrogen for 20 min) solution containing tetrabutyl ammonium hexafluorophosphate (Bu4NPF6) as the electrolyte at a constant scan rate of 50 mV/s. ITO, a Pt wire, and silver/silver chloride [Ag in 0.1 M KCl] were used as the working, counter, and reference electrodes, respectively. The electrochemical potential was calibrated against Fc/Fc+. The HOMO levels of the polymers were determined using the oxidation onset value. Onset potentials are values obtained from the intersection of the two tangents drawn at the rising current and the baseline changing current of the CV curves. TGA measurements were performed on NETZSCH TG 209 F3 thermogravimetric analyzer. All GPC analyses were made using THF as eluant and polystyrene standard as reference. X-ray diffraction (XRD) patterns were obtained using SmartLab 3 kW (40 kV 30 mA, Cu target, wavelength: 1.541871°), Rigaku, Japan. Topographic images of the active layers were obtained through atomic force microscopy (AFM) in tapping mode under ambient conditions using a XE-100 instrument. Theoretical study was performed by using density functional theory (DFT), as approximated by the B3LYP functional and employing the 6–31 G* basis set in Gaussian09.

2.2. Fabrication and characterization of polymer solar cells

All of the bulk-heterojunction PV cells were prepared using the following device fabrication procedure. The glass/indium tin oxide (ITO) substrates [Sanyo, Japan (10 Ω/γ)] were sequentially lithographically patterned, cleaned with detergent, and ultrasonicated in deionized water, acetone, and isopropyl alcohol. Then the substrates were dried on a hot-plate at 120 °C for 10 min and treated with oxygen plasma for 10 min in order to improve the contact angle just before the film coating process. Poly(3, 4-ethylene-dioxythiophene):poly(styrene-sulfonate) (PEDOT:PSS, Baytron P 4083 Bayer AG) was passed through a 0.45 μm filter before being deposited onto ITO at a thickness of *ca.* 32 nm by spin-coating at 4000 rpm in air and then it was dried at 120 °C for 20 min inside a glove box. Composite solutions with polymers and PCBM were prepared using 1,2-dichlorobenzene (DCB). The concentration was controlled adequately in the 0.5 wt% range, and the solutions were then filtered through a 0.45 μm PTFE filter and then spin-coated (500–2000 rpm, 30 s) on top of the PEDOT:PSS layer. The PFN solution in methanol and acetic acid was spin-coated on the top of the obtained active layer at 4000 rpm for 30 s to form a thin interlayer of 5 nm. The device fabrication was completed by depositing thin layers of BaF2 (1 nm), Ba (2 nm), and Al (200 nm) at pressures of less than 10–6 Torr. The active area of the device was 4.0 mm^2. Finally, the cell was encapsulated using UV-curing glue (Nagase, Japan).

The illumination intensity was calibrated using a standard a Si photodiode detector that was equipped with a KG-5filter. The output photocurrent was adjusted to match the photocurrent of the Si reference cell in order to obtain a power density of 100 mW/cm^2. After the encapsulation, all of the devices were operated under an ambient atmosphere at 25 °C. The current–voltage (*I–V*) curves of the photovoltaic devices were measured using a computer-controlled Keithley 2400 source measurement unit (SMU) that was equipped with a Peccell solar simulator under an illumination of AM 1.5 G (100 mW/cm^2). Thicknesses of the thin films were measured using a KLA Tencor Alpha-step 500 surface profilometer with an accuracy of 1 nm.

2.3. Materials

All reagents were purchased from Aldrich, Acros or TCI companies. All chemicals were used without further purification. The following compounds were synthesized following modified literature procedures: poly[quinacridone-*alt*-benzothiadiazole] (PQCDTB) [18], poly[quinacridone-*alt*-6,7-bis(octyloxy)quinoxaline] (PQCDTQ-a) [19], 5,8-bis(5-bromothiophen-2-yl)-2,3-bis(4-(octyloxy)phenyl)quinoxaline M4 [6].

2.3.1 Poly[quinacridone-alt-6,7-bis(octyloxy)quinoxaline] (PQCDTQ-b)

5,8-Bis(5-bromothiophen-2-yl)-2,3-bis(4-(octyloxy)phenyl)quinoxaline(M4) (0.23 g, 0.27 mmol), 2,9-diboronic ester-*N*,*N*0-di(2-octyl-dodecyl)quinacridone (M1) (0.30 g, 0.27 mmol), $Pd(PPh_3)_4(0)$ (0.009 g, 0.008 mmol) and Aliquat 336 were placed in a Schlenk tube, purged with three nitrogen/vacuum cycles, and under a nitrogen atmosphere added 2 M degassed aqueous K_2CO_3 (10 ml) and dry toluene (20 ml). The mixture was heated to 90 °C and stirred in the dark for 24 h. After the polymerization was over, the polymer was end-capped with bromothiophene. After reaction quenching, the whole mixture was poured into methanol. The precipitate was filtered off and purified by Soxhlet extraction with solvents in the order methanol, acetone and chloroform. The polymer was recovered from the chloroform fraction and precipitated into methanol. The final product was obtained as a dark violet solid after drying in vacuum (0.23 g, 51%). ^{1}H NMR ($CDCl_3$) *d* (ppm): 9.2–8.8 (br, 4H), 8.11 (br, 2H), 7.93 (br, 4H), 7.74 (br, 6H), 7.0–7.25 (6H), 6.83 (2H), 4.29 (br, 4H) 4.01 (br, 4H), 2.23 (br, 2H), 1.57–1.1 (br, 88H), 0.83 (br, 18H). Anal. calcd. for: $C_{104}H_{140}N_4O_4S_2$: C, 79.34; H, 8.96; N, 3.56; O, 4.06; S, 4.07. Found: C, 79.22; H, 9.03; N, 3.56; O, 4.09; S, 4.05%.

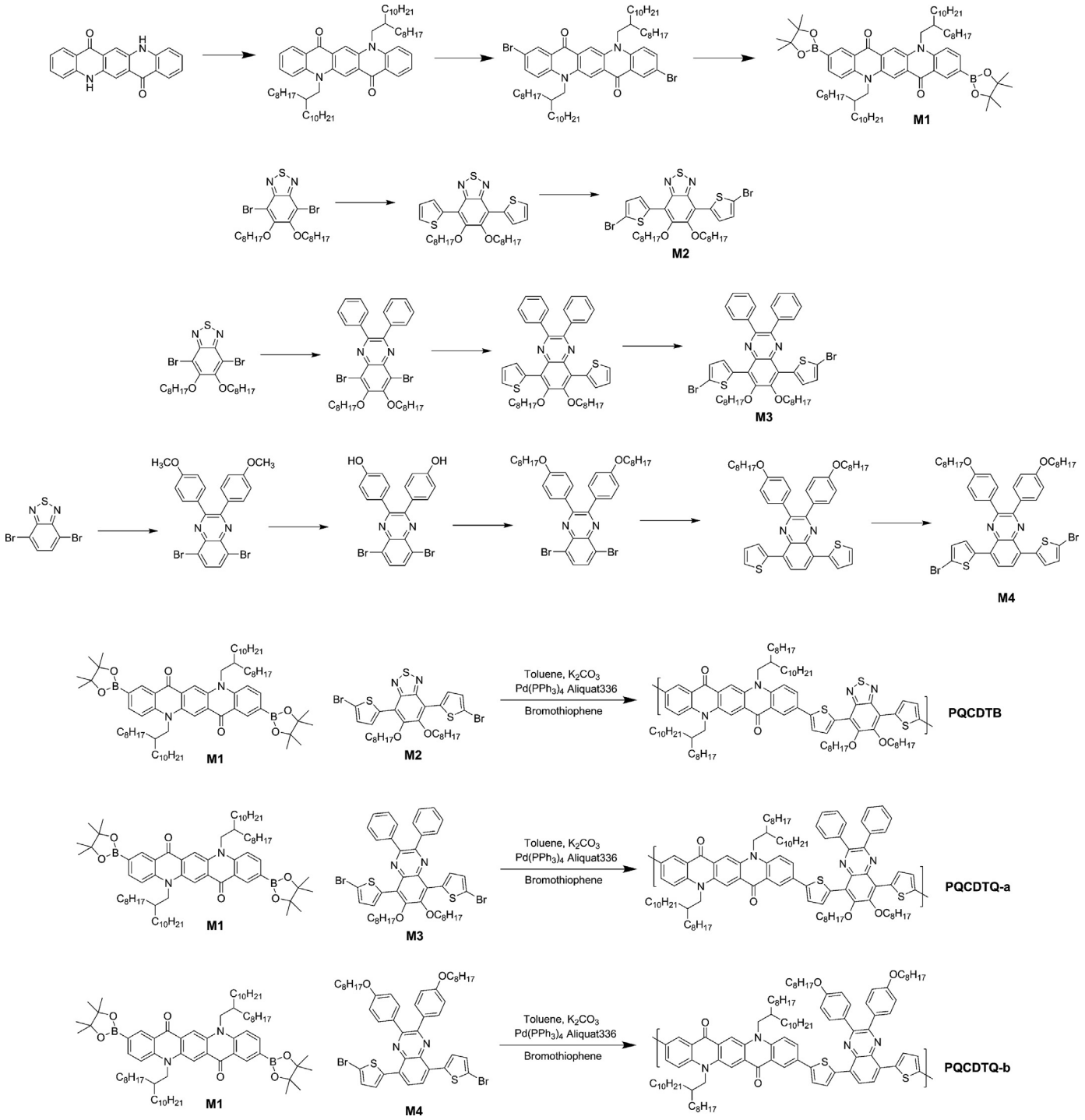

Scheme 1. Monomer synthesis and polymerization.

3. Results and discussion

3.1. Synthesis and characterization of the polymers

Scheme 1 presents the chemical structure and synthetic process for both the monomer and polymer. All of the polymers were synthesized through the Suzuki coupling reaction using M1, M2, M3, and M4 and included poly(quinacridone-benzothiadiazole) (PQCDTB), poly(quinacridone-6,7-bis(octyloxy)-diphenylquinoxaline) (PQCDTQ-a), and poly(quinacridone-2,3-bis(octyloxy)-diphenylquinoxaline) (PQCDTQ-b). The polymerization was performed at 90 °C for 24 h with a palladium(0) catalyst, 2 M potassium carbonate solution, aliquot 336 as a surfactant, and toluene as the solvent. The polymer was end-capped with bromothiophene after the polymerization was complete. The synthesized polymer was purified with soxhlet extraction in the following order: methanol, acetone, and chloroform. The polymer was then recovered from the chloroform fraction and precipitated into methanol. As a result, the yields of PQCDTB, PQCDTQ-a, and PQCDTQ-b reached 92, 73, and 51%, respectively. The obtained polymer dissolved in organic solvents, such as THF, chloroform, chlorobenzene, and o-dichlorobenzene. A homogenous semitransparent film of red or violet was formed through spin-coating.

Table 1 lists the molecular weight and thermal properties of the polymers. When the GPC was measured using polystyrene as the standard, the number-average molecular weights (M_n) of PQCDTB, PQCDTQ-a, and PQCDTQ-b were 124.5, 67.2, and 57.9 kg/mol, respectively. In contrast, the polydispersity indices (PDIs) exhibited a distribution of 4.53, 2.83, and 3.44, respectively. The degree of polymerization in PQCDTB was higher than that in PQCDTQ-a or PQCDTQ-b, which might be due to position of alkoxy chain. PQCDTB is expected to generate a high photocurrent density compared with PQCDTQ-a and PQCDTQ-b due to its high molecular weight. Table 1 presents the results of the thermal analysis performed through TGA. PQCDTB, PQCDTQ-a, and PQCDTQ-b experienced a 5% weight loss at temperatures of 322–355 °C, respectively, indicating high thermal stability due to the rigid QC structure. This stability makes the polymers applicable to optoelectronic devices and OPVs, both of which require a thermal stability over 300 °C [18]. We investigated the thermal behavior using DSC analysis (see SI), which revealed no obvious thermal transitions in any of the polymers in the temperature range of 40–250 °C.

3.2. Optical and electrochemical properties

Fig. 1(a) and (b) presents the UV–visible (UV–vis) spectra of the polymers in solution and of the thin-film polymers. The maximum absorption peaks of PQCDTB (λ_{max}) were observed at 393 and 539 nm in solution (10^{-6} M in chloroform). In contrast, the maximum absorption peaks of PQCDTQ-a and PQCDTQ-b (λ_{max}) were observed at 388, 537, and 584 nm and at 393 and 536 nm in solution, respectively. The band at approximately 350–400 nm in the absorption spectra of the polymers was assigned to the $\pi-\pi^*$ transition, whereas the 530 – 600 nm band occurred due to ICT between the donor and acceptor moieties [10]. The absorption spectrum of PQCDTQ-b near 550–650 nm was broadened and red-shifted compared with those of PQCDTB and PQCDTQ-a, which can be explained by the ICT effects that are much stronger in PQCDTQ-b than those in PQCDTB and PQCDTQ-a due to the position of the oxygen atom. The maximum absorption spectra of the polymers in the film were red-shifted compared with those in the solution. These results were explained by their more planar conformations in the solid state. Notably, all of the thin-film polymers exhibited

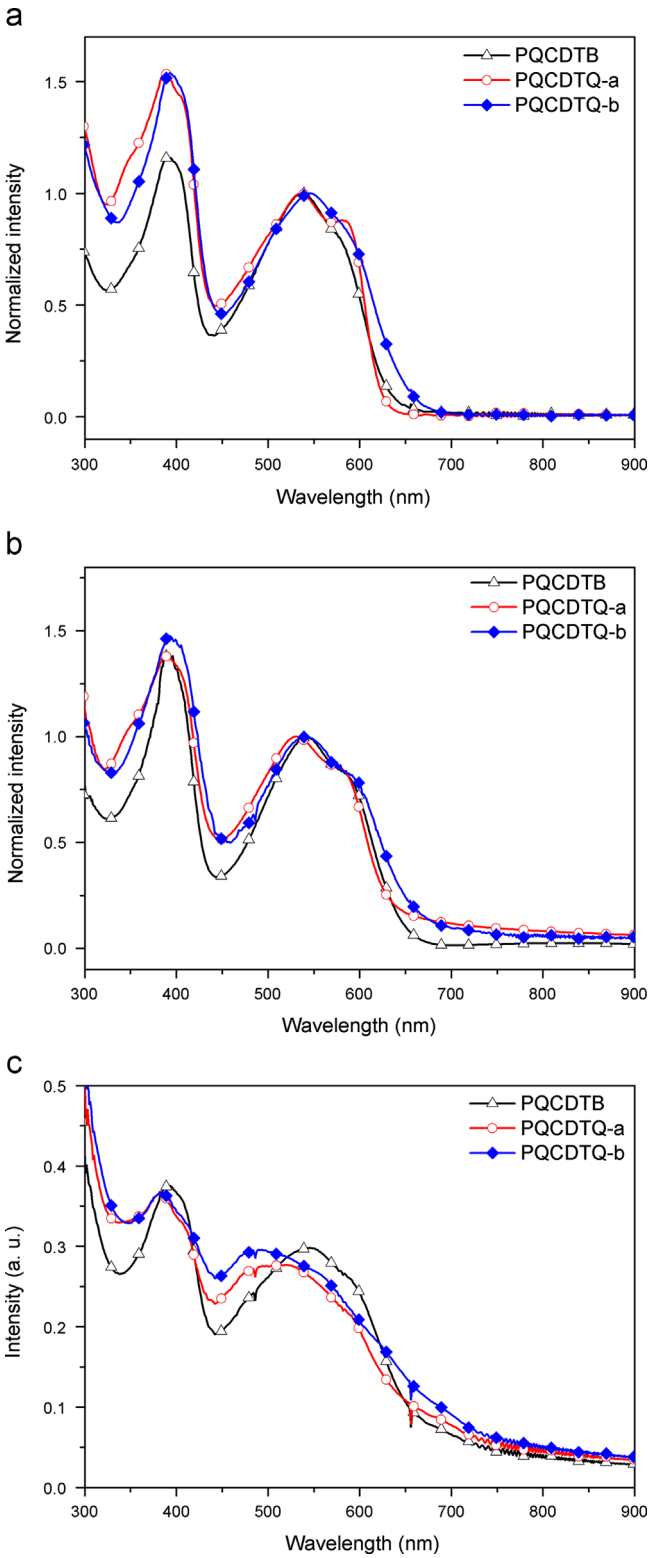

Fig. 1. Absorption spectra of polymers in (a) solution (10^{-6} M), (b) film (50 nm) and (c) polymer:$PC_{71}BM$ blend film (50–60 nm).

Table 1
Molecular weight and thermal properties of the polymers.

Polymer	M_n (kg/mol)	M_w (kg/mol)	PDI	T_d (°C)
PQCDTB	40.5	482.9	11.9	323
PQCDTQ-a	47.2	246.8	5.22	346
PQCDTQ-b	63.1	321.6	5.09	355

a shoulder absorption peak near 580 nm, which indicates that these polymers may have a more ordered structure in the solid form [22]. The calculated optical band gaps of PQCDTB, PQCDTQ-a, and PQCDTQ-b through the UV onset value of the film were 1.92, 1.97, and 1.90 eV, respectively.

Fig. 1(c) presents the UV–vis spectra of the spin-coated blend film with polymer and phenyl-C71-butyric acid methyl ester ($PC_{71}BM$) (thickness: 50 nm). The absorption spectrum of PQCDTQ-b exhibited a somewhat broad intensity compared with that of PQCDTQ-a. PQCDTB exhibited strong absorption intensity near 530–630 nm compared with PQCDTQ-a and PQCDTQ-b, which was caused by high absorption coefficient of PQCDTB. The result that PQCDTB exhibits a higher photocurrent density might be expected.

Fig. 2 presents the cyclic voltammograms of polymers, which were measured in 0.1 M tetrabutylammonium-hexafluorophosphate acetonitrile under a nitrogen atmosphere. A clear oxidation–reduction peak was observed in all of the polymers because the polymers were D–A structured, unlike the PQA2T (poly[quinacridone-bithiophene]) of typical p-type structure reported by Takimiya et al. [17]. The oxidations (E_{ox}^{onset}) of the PQCDTB, PQCDTQ-a, and PQCDTQ-b were +0.90, 0.99, and 0.80 V, respectively, and the HOMO levels were calculated to be −5.28, −5.37, and −5.18 eV, respectively. The HOMO levels of PQCDTB and PQCDTQ-a exhibited similar values reported in our research [18,19]. The optical and electrochemical properties of the polymers are summarized in Table 2. Because the HOMO levels of PQCDTQ-a are lower than those of PQCDTB and PQCDTQ-b, a relatively high air stability and V_{OC} were obtained. Notably, the polymers based on the quinoxaline derivative exhibited different HOMO levels depending on the octyloxy chain position. The HOMO level of PQCDTQ-b (−5.18 eV) was higher than that of PQCDTQ-a (−5.28 eV), which was caused by the oxygen of the electron-deficient group around the polymer backbone. The LUMO energy levels were calculated from the difference between the HOMO energy levels and optical band gap energies. According to these calculations, the LUMO levels of PQCDTB, PQCDTQ-a, and PQCDTQ-b were −3.36, −3.40, and −3.28 eV, respectively.

Fig. 3 presents the band diagram of the energy levels obtained through CV measurement and the HOMO and LUMO distributions obtained using density functional theory (DFT) calculations in Gaussian at the B3LYP/6–31G* level. As observed in Fig. 3, the LUMO level of PQCDTQ-a (−3.40 eV) was lower than those of PQCDTB and PQCDTQ-b (−3.36 and −3.28 eV, respectively) by 0.12 eV. Therefore, if charge separation occurred after receiving light energy, an electron in PQCDTQ-a would exhibit more effective charge transport to PCBM than an electron in PQCDTB or PQCDTQ-b in the active layer [14].

As demonstrated in the HOMO and LUMO distributions of the polymers, the LUMO orbital of PQCDTQ-a was partially located on

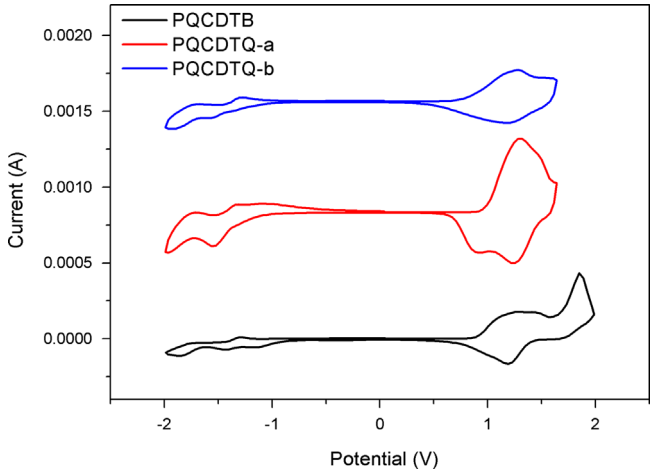

Fig. 2. Cyclic voltammogram of polymers with a 0.1 M acetonitrile (substituted with nitrogen for 5 min) solution.

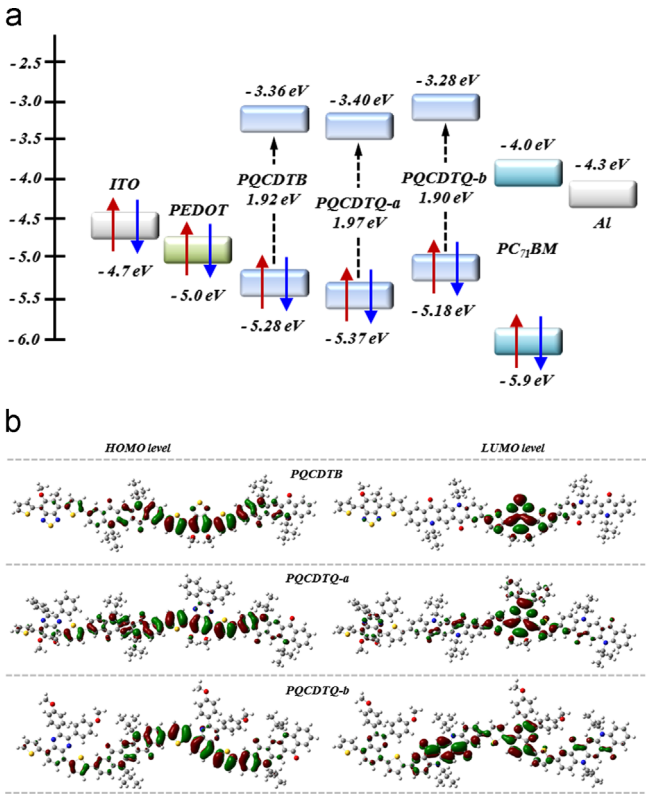

Fig. 3. DFT Gaussian simulation and band diagram of polymers (experiment level), ITO, $PC_{71}BM$, Al.

Table 2
Optical and electrochemical properties of the polymers.

Polymer	Absorption, λ_{max} (nm)		E_{ox}^{onset} (V)	E_{HOMO} (eV)[c]	E_{LUMO} (eV)[d]	E_{opt} (eV)[e]
	Solution[a]	Film[b]				
PQCDTB	393, 539	391, 540	0.90	−5.28	−3.36	1.92
PQCDTQ-a	388, 537, 584	389, 531, 578	0.99	−5.37	−3.40	1.97
PQCDTQ-b	393, 546	393, 538, 579	0.80	−5.18	−3.28	1.90

[a] Absorption spectrum in $CHCl_3$ solution (10^{-6} M).
[b] Spin-coated thin film (50 nm).
[c] Calculated from the oxidation onset potentials under the assumption that the absolute energy level of Fc/Fc+ was −4.8 eV below a vacuum.
[d] HOMO − E_{opt}.
[e] Estimated from the onset of UV–vis absorption data of the thin film.

the donor QC derivative, which suggested an incomplete ICT effect. In contrast, the LUMO orbitals of PQCDTB were located mostly on the acceptor benzothiadizole derivative, which suggested a strong ICT effect [5,19]. Notably, for PQCDTQ-b, the electron densities of the HOMO and LUMO are both well delocalized over the conjugated repeat unit (both the acceptor and donor). The extensive

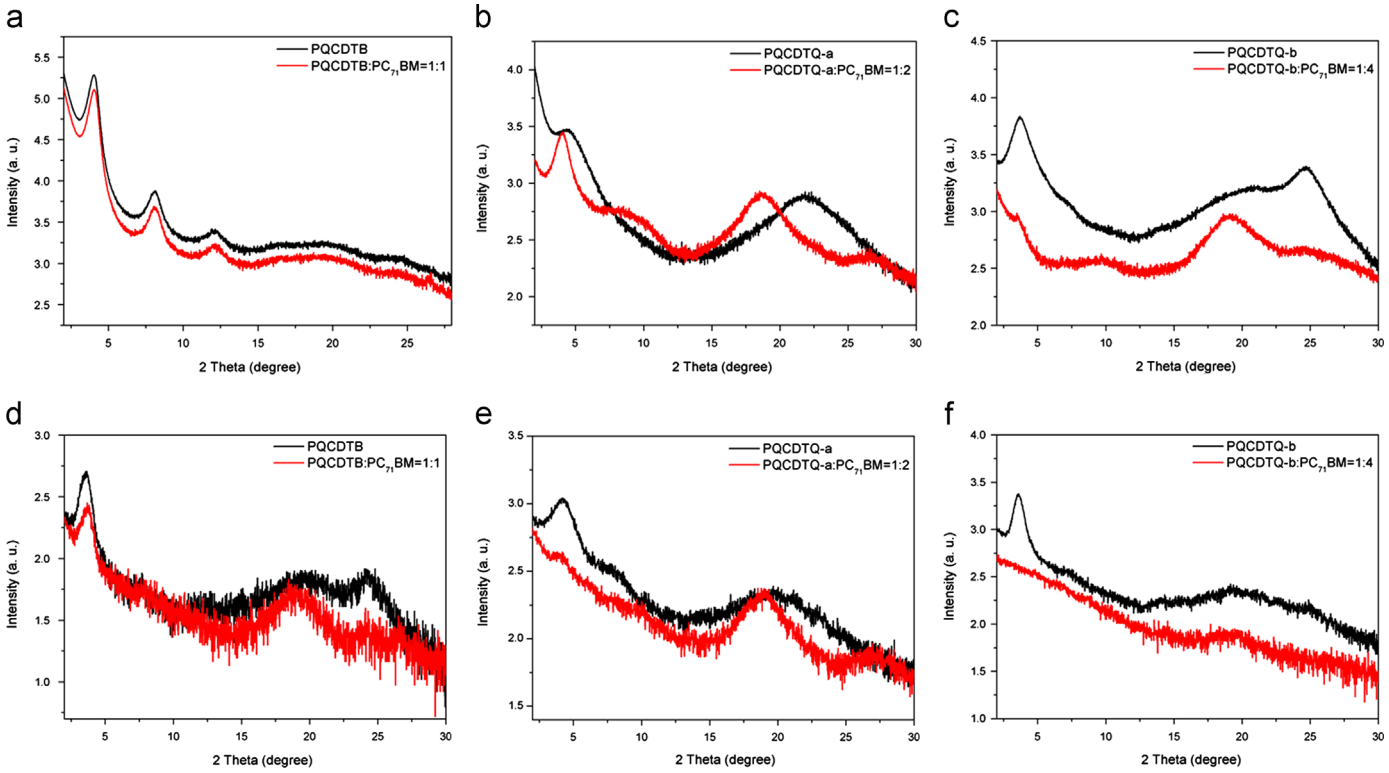

Fig. 4. (a–c) Out-of-plane and (d–f) in-plane in X-ray diffraction pattern in thin films after thermal treatment.

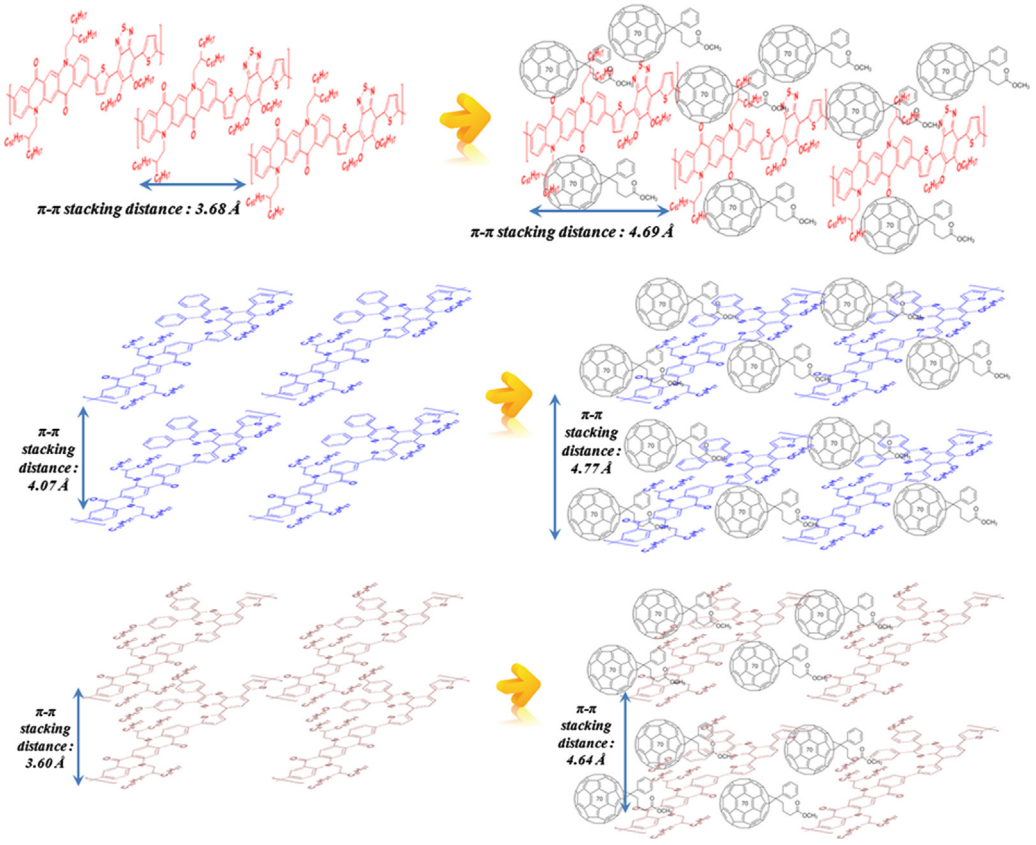

Fig. 5. Schematic representation of intercalated packing structure between polymer and $PC_{71}BM$.

delocalization of both the HOMO and LUMO may partly explain the robust ambipolar behavior observed [23].

3.3. Orientation analysis

Figs. 4 and 5 present X-ray diffraction (XRD) measurements and a schematic representation of the film used to analyze the ordering structure of the polymers and $PC_{71}BM$. As observed in Fig. 4(a), sharp diffraction peaks were present at 4.0° in the out-of-plane peak of both PQCDTB and the PQCDTB:$PC_{71}BM$ blend, indicating the formation of an ordered lamellar structure as an out-of-plane peak (100) by the alkyl side chain of quinacridone and conventional edge-on π-stacking [17,18]. However, as observed in Fig. 4(d), in the (010) in-plane patterns, the d_π-spacings related to π–π stacking were changed. The d_π-spacing with only PQCDTB was 3.68 Å, whereas the d_π-spacing with the PQCDTB:$PC_{71}BM$ blend increased to 4.69 Å. The distance of $\pi-\pi$ stacking increased with the size of $PC_{71}BM$ because $PC_{71}BM$ intercalated among the alkyl chains of PQCDTB, as observed in Fig. 5(a). As observed in Fig. 4 (b) and (c), the (010) diffraction corresponding to π–π stacking was more prominent in the out-of-plane pattern of PQCDTQ-a and PQCDTQ-b. This result suggested that a large fraction of the PQCDTQ-a and PQCDTQ-b backbones were oriented face-on relative to the substrate due to the phenyl ring structure of the quinoxaline derivative. For the polymer:$PC_{71}BM$ blends, the d_π-spacings of PQCDTQ-a and PQCDTQ-b increased to 4.77 and 4.64 Å, respectively, compared with only the polymer. This result was due to the same reason as that for the PQCDTB:$PC_{71}BM$ blend.

For only the polymer, the d_π-spacings of PQCDTB and PQCDTQ-b (3.68 and 3.60 Å, respectively) indicated a short π–π stacking distance compared with PQCDTQ-a (4.07 Å). However, for the polymer:$PC_{71}BM$ blends, all of the polymers had similar π–π stacking distances (4.69, 4.77, and 4.64 Å). Among these blends, the PQCDTQ-b:$PC_{71}BM$ blend exhibited the smallest π–π stacking distance and face-on orientation, which was expected because this blend exhibited the best fill factor (FF) by low series resistance [18].

The tilt angles were comparatively analyzed by calculating the PQCDTB, PQCDTQ-a, and PQCDTQ-b configurations using DFT calculations. Overall, the tilt angles of PQCDTB and PQCDTQ-b (13–24°) were lower compared with those of PQCDTQ-a (18–22°). Thus, it was suggested that π–π stacking was more effective in PQCDTB and PQCDTQ-b than in PQCDTQ-a. This result is consistent with the aforementioned XRD results. PQCDTB and PQCDTQ-b (3.68 and 3.60 Å, respectively) exhibited shorter π–π stacking distances than PQCDTQ-a (4.07 Å).

3.4. Photovoltaic characteristics

Fig. 6 and Table 3 present the results of an evaluation of OPV device characteristics. The devices were structured as follows: ITO (170 nm)/PEDOT:PSS (40 nm)/active layer (50 nm)/PFN (5 nm)/Al (100 nm). The active layer had an optimized blending ratio obtained by dissolving the polymer and $PC_{71}BM$ in chlorobenzene (CB) with 1,8-diiodootane (DIO) of 3 vol% using a concentration of approximately 0.5–1 wt%. The spin-cast film was slow dried in a vacuum and annealed at 120 °C for 10 min.

The V_{OC}, short-circuit current (J_{SC}), FF, and PCE were 0.77 V, 8.0 mA/cm^2, 47.0%, and 2.9%, respectively, for PQCDTB with a 1:1 ratio of $PC_{71}BM$ (50 nm thick). Compared with reported device structure, the device of PQCDTB with DIO showed improved J_{SC} (42%) and PCE (16%) [18]. For the device with PFN, a PCE of 3.8% and an increased FF of 12.7% were reported compared with the device without PFN. The PQCDTB device exhibited the most improved FF compared with the other polymers. This result occurred because PFN changed from a rough to smooth surface due to the edge-on orientation of PQCDTB. The PQCDTB device

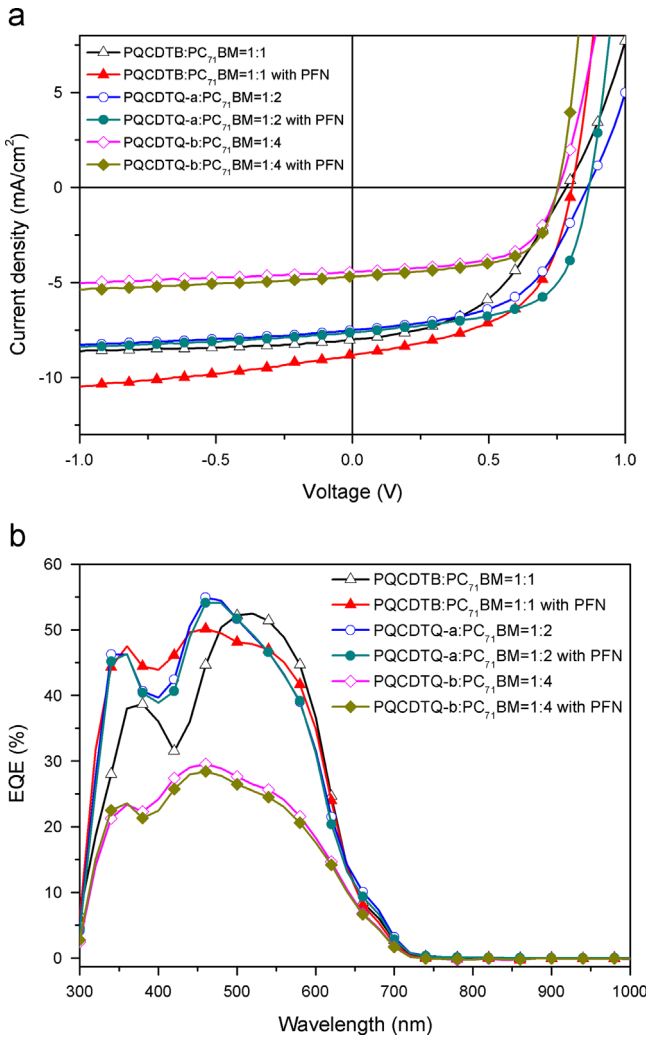

Fig. 6. (a) *J–V* characteristics (b) EQE spectra of the BHJ solar cells with the device.

exhibited the highest photocurrent density (8.0 mA/cm^2 *vs.* 7.5, 4.4 mA/cm^2) because PQCDTB absorbed more photons due to broad absorption near 530–630 nm, as indicated in the UV–vis spectra (Fig. 1(c)).

The V_{OC}, J_{SC}, FF, and PCE were 0.85 V, 7.5 mA/cm^2, 53.4%, and 3.4%, respectively, for PQCDTQ-a with a 1:2 ratio of $PC_{71}BM$. For the device with PFN, a PCE of 4.0% and an increased FF of 8.1% were reported compared with the device without PFN. The PQCDTQ-a device exhibited the best performance, with a high V_{OC} and FF that occurred due to the low HOMO level (−5.37 eV) and face-on orientation compared with PQDTB and PQCDTQ-b. In addition, the PQCDTQ-a device exhibited improved performance (PCE=4.0%) compared with previously reported performance (3.6%) because the slow, dry treatment in the vacuum condition formed a stable surface [24].

The V_{OC}, J_{SC}, FF, and PCE were 0.75 V, 4.4 mA/cm^2, 59.8%, and 2.0%, respectively, for PQCDTQ-b with a 1:4 ratio of $PC_{71}BM$. For the device with PFN, a PCE of 2.2% and a somewhat increased FF were reported. The Voc of PQCDTQ-b was somewhat lower than that of the other polymers (0.75 V *vs.* 0.79 and 0.85 V) because the PQCDTQ-b had higher HOMO levels than the other polymers (−5.18 eV *vs.* −5.28 and −5.37 eV).

For devices without PFN, PQCDTQ-b exhibited a higher FF than PQCDTB and PQCDTQ-a (59.8% *vs.* 47.0 and 53.4%) because the π–π stacking distance of PQCDTQ-b:$PC_{71}BM$ (4.64 Å) was shorter than that of PQCDTB:$PC_{71}BM$ (4.77 Å). In addition, the π–π stacking

Table 3
Photovoltaic performance of the BHJ solar cells with the device.

Active layer (w/w) Polymer:$PC_{71}BM$	Weight ratio (P:A, w/w)	V_{OC} (V)	J_{SC} (mA/cm^2)	FF (%)	PCE (%)
PQCDTB	1:1	0.77	8.0	47.0	2.9
	1:1 with PFN	0.79	8.0	59.7	3.8
PQCDTQ-a	1:2	0.85	7.5	53.4	3.4
	1:2 with PFN	0.85	7.6	61.5	4.0
PQCDTQ-b	1:4	0.75	4.4	59.8	2.0
	1:4 with PFN	0.75	4.7	60.9	2.2

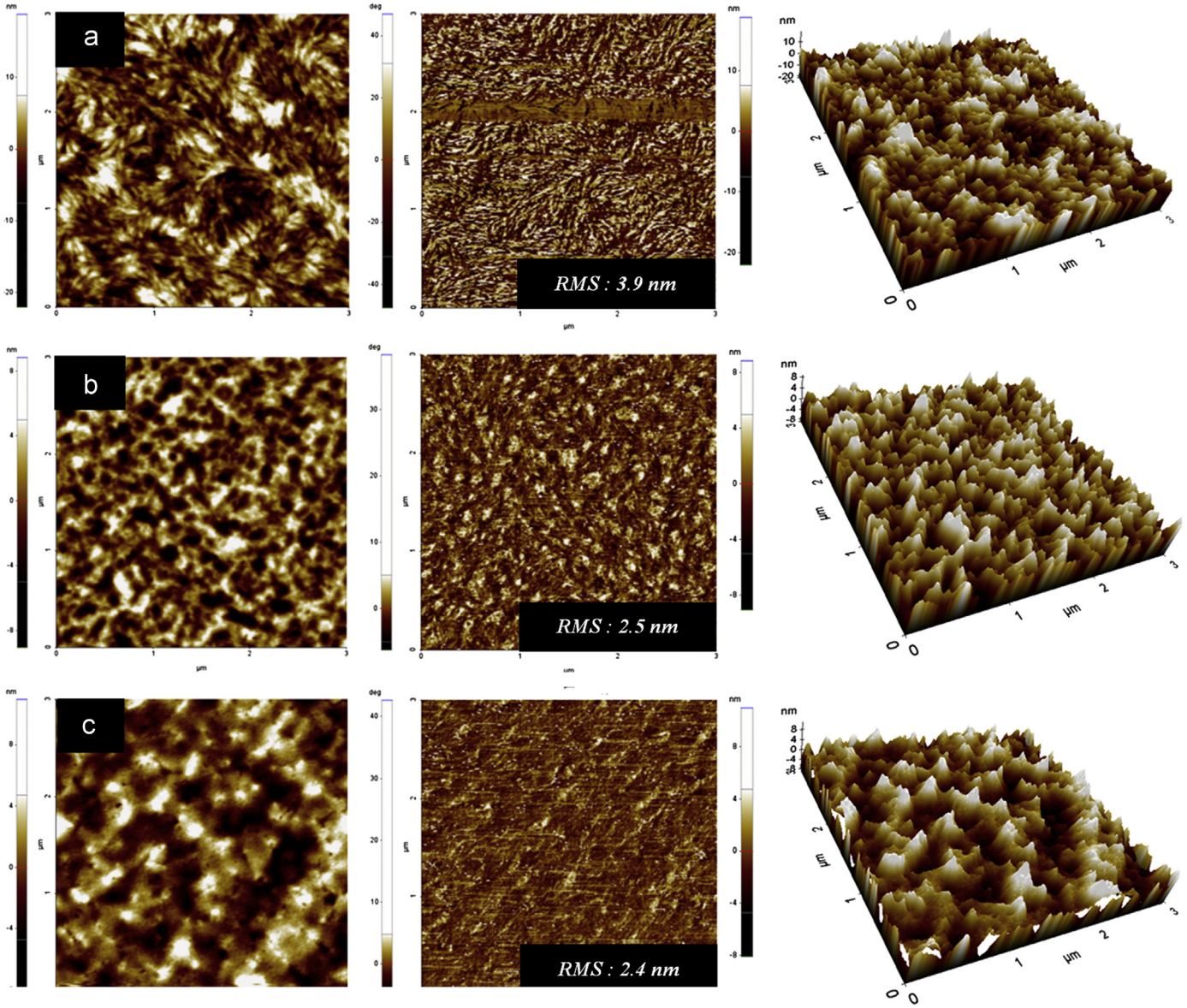

Fig. 7. Topographic AFM images of (a) PQCDTB:$PC_{71}BM$ 1:1, (b) PQCDTQ-a:$PC_{71}BM$ 1:2, and (c) PQCDTQ-b:$PC_{71}BM$ 1:4.

distance of PQCDTB:$PC_{71}BM$ (4.69 Å) is similar to that of PQCDTQ-b:$PC_{71}BM$; however, the orientation of PQCDTB:$PC_{71}BM$ has an edge-on structure. Thus, the fact that the edge-on orientation does not have more effective electron transport related to the π–π stacking direction than to the face-on orientation suggests that PQCDTQ-b exhibits a higher FF than PQCDTB.

As observed in Fig. 1, the ICT effect of PQCDTQ-b was much stronger than that of other polymers. However, unexpectedly, PQCDTQ-b exhibited a lower current density than PQCDTQ-a (4.4 mA/cm^2 *vs.* 7.5 mA/cm^2) due to the morphology of the macro-phase separation, as shown in Fig. 7(c).

To verify the accuracy of the device measurements, their external quantum efficiencies (EQEs) were measured, and the EQE curve, including its ratio to $PC_{71}BM$, is presented in Fig. 6(b). The photons in the EQE curve occurred mainly in the polymer phase, which correlated with the absorption spectra of the

polymers [25]. The EQE curve is similar to the UV–vis spectra curve in Fig. 1. PQCDTB absorbed more photons due to broad absorption near 530–630 nm, as indicated in the UV–vis spectra (Fig. 1(c)).

3.5. Morphology analysis

Atomic force microscopy (AFM) was used to investigate the morphology of the polymer/$PC_{71}BM$ blend film, and the results are presented in Fig. 7. As observed in Fig. 7(a), PQCDTB formed a small fibril-type domain at a 1:1 PQCDTB/$PC_{71}BM$ ratio. PQCDTB/$PC_{71}BM$ blend film with DIO showed similar topology with only PQCDTB/$PC_{71}BM$ blend film [18], which suggests that DIO have a strong influence on absorption of photocurrent than morphology. It appears that this type of fibril domain occurred because PQCDTB formed an edge-on structure on the substrate. Micro-phase separation occurred between PQCDTQ-a and $PC_{71}BM$, as observed in Fig. 7(b), and the PQCDTQ-a formed a hive-shaped network at a 1:2 PQCTQx/$PC_{71}BM$ ratio. In contrast, when the PQCDTQ-b/$PC_{71}BM$ ratio was 1:4, PQCDTQ-b assembled as illustrated in Fig. 6(a), and a large domain with a length of 0.5–1 μm was formed. A relatively large phase separation occurred as a result. The large phase separation exhibited a low photocurrent by reducing the charge separation and increasing the exciton diffusion length and recombination of electric charges [26]. The same results are confirmed for the current device using the data in Table 3.

4. Conclusions

In this study, quinacridone-acceptor series were successfully synthesized using the Suzuki coupling reaction by introducing a planar quinacridone unit and a highly soluble acceptor unit. The polymers exhibited high molecular weights and good thermal stability. The ICT effects were much stronger in PQCDTQ-b than in PQCDTB and PQCDTQ due to the position of the oxygen atom. According to the XRD measurements, PQCDTB formed an ordered lamellar structure and displayed conventional edge-on π-stacking. In contrast, PQCDTQ-a and PQCDTQ-b formed a face-on structure relative to the substrate. PQCDTQ-b exhibited the shortest π–π stacking distance, which resulted in the highest FF in the device. For the device with PFN, the V_{OC}, J_{SC}, FF, and PCE of PQCDTQ-a with a 1:2 ratio of $PC_{71}BM$ were 0.85 V, 7.6 mA/cm^2, 61.5%, and 4.0%, respectively, due to the face-on orientation and micro-phase separation compared with PQCDTB and PQCDTQ-b. Unexpectedly, PQCDTQ-b exhibited a lower current density than PQCDTQ-a due to the morphology of the macro-phase separation. It is likely that more effective performance levels could be obtained if the morphology and various additives for the PQCDTQ-b were optimized.

Acknowledgments

This research was supported by a grant from the Fundamental R&D Program for Core Technology of Materials funded by the Ministry of Knowledge Economy, Republic of Korea (10037195). This work was supported by the National Research Foundation of Korea Grant funded by the Korean Government (MEST) (NRF-2009-C1AAA001-2009-0093526).

Appendix A. Supporting information

Supplementary data associated with this article can be found in the online version at http://dx.doi.org/10.1016/j.solmat.2013.12.004.

References

[1] R.H. Friend, R.W. Gymer, A.B. Holmes, J.H. Burroughes, R.N. Marks, C. Taliani, D.D.C. Bradley, D.A.D. Santos, J.L. Bredas, M. Logdlund, W.R. Salaneck, Electroluminescence in conjugated polymers, Nature 397 (1999) 121–128.
[2] C.A. Breen, J.R. Tischler, V. Bulović, T.M. Swager, Highly efficient blue electroluminescence from poly(phenylene ethynylene) via energy transfer from a hole-transport matrix, Adv. Mater. 17 (2005) 1981–1985.
[3] H.J. Song, J.Y. Lee, I.S. Song, D.K. Moon, J.R. Haw, Synthesis and electroluminescence properties of fluorene–anthracene based copolymers for blue and white emitting diodes, J. Ind. Eng. Chem. 17 (2011) 352–357.
[4] F.C. Krebs, Polymer solar cell modules prepared using roll-to-roll methods: knife-over-edge coating, slot-die coating and screen printing, Solar Energy Mater. Solar Cells 93 (2009) 465–475.
[5] S. Subramaniyan, H. Xin, F.S. Kim, S. Shoaee, J.R. Durrant, S.A. Jenekhe, Effects of side chains on thiazolothiazole-based copolymer semiconductors for high performance solar cells, Adv. Energy Mater. 1 (2011) 854–860.
[6] J.-Y. Lee, S.-H. Kim, I.-S. Song, D.-K. Moon, Efficient donor-acceptor type polymer semiconductors with well-balanced energy levels and enhanced open circuit voltage properties for use in organic photovoltaics, J. Mater. Chem. 21 (2011) 16480–16487.
[7] M. Manceau, D. Angmo, M. Jørgensen, F.C. Krebs, ITO-free flexible polymer solar cells: from small model devices to roll-to-roll processed large modules, Org. Electron. 12 (2011) 566–574.
[8] M.O. Reese, S.A. Gevorgyan, M. Jørgensen, E. Bundgaard, S.R. Kurtz, D.S. Ginley, D.C. Olson, M.T. Lloyd, P. Morvillo, E.A. Katz, A. Elschner, O. Haillant, T.R. Currier, V. Shrotriya, M. Hermenau, M. Riede, K.R. Kirov, G. Trimmel, T. Rath, O. Inganäs, F. Zhang, M. Andersson, K. Tvingstedt, M. Lira-Cantu, D. Laird, C. McGuiness, S. Gowrisanker, M. Pannone, M. Xiao, J. Hauch, R. Steim, D.M. De Longchamp, R. Rösch, H. Hoppe, N. Espinosa, A. Urbina, G. Yaman-Uzunoglu, J.-B. Bonekamp, A.J.J.M. van Breemen, C. Girotto, E. Voroshazi, F.C. Krebs, Consensus stability testing protocols for organic photovoltaic materials and devices, Sol. Energy Mater. Sol. Cells 95 (2011) 1253–1267.
[9] F.C. Krebs, J. Fyenbo, M. Jorgensen, Product integration of compact roll-to-roll processed polymer solar cell modules: methods and manufacture using flexographic printing, slot-die coating and rotary screen printing, J. Mater. Chem. 20 (2010) 8994–9001.
[10] Y. Zhu, R.D. Champion, S.A. Jenekhe, Conjugated donor – acceptor copolymer semiconductors with large intramolecular charge transfer: synthesis, optical properties, electrochemistry, and field effect carrier mobility of thienopyrazine-based copolymers, Macromolecules 39 (2006) 8712–8719.
[11] J. Kuwabara, Y. Nohara, S.J. Choi, Y. Fujinami, W. Lu, K. Yoshimura, J. Oguma, K. Suenobu, T. Kanbara, Direct arylation polycondensation for the synthesis of bithiophene-based alternating copolymers, Polym. Chem. 4 (2013) 947–953.
[12] J. Mei, D.H. Kim, A.L. Ayzner, M.F. Toney, Z. Bao, Siloxane-terminated solubilizing side chains: bringing conjugated polymer backbones closer and boosting hole mobilities in thin-film transistors, J. Am. Chem. Soc. 133 (2011) 20130–20133.
[13] C.-J. Lin, W.-Y. Lee, C. Lu, H.-W. Lin, W.-C. Chen, Biaxially extended thiophene-fused thiophene conjugated copolymers for high performance field effect transistors, Macromolecules 44 (2011) 9565–9573.
[14] J.-M. Jiang, P.-A. Yang, T.-H. Hsieh, K.-H. Wei, Crystalline low-band gap polymers comprising thiophene and 2,1,3-benzooxadiazole units for bulk heterojunction solar cells, Macromolecules 44 (2011) 9155–9163.
[15] S. De Feyter, A. Gesquière, F.C. De Schryver, U. Keller, K. Müllen, Aggregation properties of soluble quinacridones in two and three dimensions, Chem. Mater. 14 (2001) 989–997.
[16] X. Yang, J. Wang, X. Zhang, Z. Wang, Y. Wang, Stm study on 2d molecular assemblies of luminescent quinacridone derivatives: structure fine-tuned by introducing bulky substitutes and co-adsorption with monofunctional/bifunctional acid, Langmuir 23 (2006) 1287–1291.
[17] I. Osaka, M. Akita, T. Koganezawa, K. Takimiya, Quinacridone-based semiconducting polymers: implication of electronic structure and orientational order for charge transport property, Chem. Mater. 24 (2012) 1235–1243.
[18] H.-J. Song, D.-H. Kim, E.-J. Lee, S.-W. Heo, J.-Y. Lee, D.-K. Moon, Conjugated polymer consisting of quinacridone and benzothiadiazole as donor materials for organic photovoltaics: coplanar property of polymer backbone, Macromolecules 45 (2012) 7815–7822.
[19] H.-J. Song, D.-H. Kim, E.-J. Lee, D.-K. Moon, Conjugated polymers consisting of quinacridone and quinoxaline as donor materials for organic photovoltaics: orientation and charge transfer properties of polymers formed by phenyl structures with a quinoxaline derivative, J. Mater. Chem. A 1 (2013) 6010–6020.
[20] H. Yi, S. Al-Faifi, A. Iraqi, D.C. Watters, J. Kingsley, D.G. Lidzey, Carbazole and thienyl benzo[1,2,5]thiadiazole based polymers with improved open circuit voltages and processability for application in solar cells, J. Mater. Chem. 21 (2011) 13649–13656.
[21] Y. Huang, M. Zhang, L. Ye, X. Guo, C.C. Han, Y. Li, J. Hou, Molecular energy level modulation by changing the position of electron-donating side groups, J. Mater. Chem. 22 (2012) 5700–5705.
[22] Y. Li, J. Zou, H.-L. Yip, C.-Z. Li, Y. Zhang, C.-C. Chueh, J. Intemann, Y. Xu, P.-W. Liang, Y. Chen, A.K.Y. Jen, Side-chain effect on cyclopentadithiophene/fluorobenzothiadiazole-based low band gap polymers and their applications for polymer solar cells, Macromolecules 46 (2013) 5497–5503.

[23] R.S. Ashraf, A.J. Kronemeijer, D.I. James, H. Sirringhaus, I. McCulloch, A new thiophene substituted isoindigo based copolymer for high performance ambipolar transistors, Chem. Commun. 48 (2012) 3939–3941.
[24] R. Lin, M. Wright, A. Uddin, Effects of solvent additive on inverted structure pcpdtbt:Pc71bm bulk heterojunction organic solar cells, Phys. Status Solidi (a) 210 (2013) 1785–1790.
[25] A. Gadisa, W. Mammo, L.M. Andersson, S. Admassie, F. Zhang, M.R. Andersson, O. Inganäs, A new donor–acceptor–donor polyfluorene copolymer with balanced electron and hole mobility, Adv. Funct. Mater. 17 (2007) 3836–3842.
[26] E. Wang, L. Hou, Z. Wang, Z. Ma, S. Hellström, W. Zhuang, F. Zhang, O. Inganäs, M.R. Andersson, Side-chain architectures of 2,7-carbazole and quinoxaline-based polymers for efficient polymer solar cells, Macromolecules 44 (2011) 2067–2073.